Am J Nucl Med Mol Imaging 2025;15(4):130-139
www.ajnmmi.us /ISSN:2160-8407/ajnmmi0166980

Original Article

Dual-receptor PET imaging of ovarian cancer using a ^{68}Ga-labeled heterodimer targeting folate receptor and HER2

Xiaodan Shi[1,2], Zhangxin Wu[1,2], Yifeng Yuan[1,2], Ying Wang[1,2], Shuo Yang[1,2], Rong Li[1,2]

[1]State Key Laboratory of Female Fertility Promotion, National Clinical Research Center for Obstetrics and Gynecology, Key Laboratory of Assisted Reproduction (Ministry of Education), Beijing Key Laboratory of Reproductive Endocrinology and Assisted Reproductive Technology, Center for Reproductive Medicine, Department of Obstetrics and Gynecology, Peking University Third Hospital, Beijing 100191, China; [2]National Clinical Key Specialty Construction Program, Peking University Third Hospital, Beijing 100191, China

Received June 22, 2025; Accepted August 3, 2025; Epub August 15, 2025; Published August 30, 2025

Abstract: Radiolabeled folate derivatives have been extensively investigated for positron emission tomography (PET) imaging of ovarian cancer due to the frequent overexpression of folate receptor α (FRα). However, clinical translation has been hindered, at least in part, by suboptimal tumor uptake of FRα-targeted radiotracers. In this study, we developed and characterized a ^{68}Ga-labeled heterodimeric radiotracer, ^{68}Ga-folate-KR, designed to concurrently target FRα and human epidermal growth factor receptor 2 (HER2), another receptor commonly overexpressed in ovarian cancer. Transcriptomics analysis confirmed the co-upregulation of *FOLR1* and *HER2* in ovarian cancer tissues relative to normal ovarian tissue, supporting the rationale for dual-receptor targeting. In vitro binding assays demonstrated specific binding of ^{68}Ga-folate-KR to both receptors. PET imaging and biodistribution studies in SKOV3 tumor-bearing mice revealed significantly enhanced tumor uptake and improved tumor-to-nontumor contrast compared to the monomeric radiotracers ^{68}Ga-folate and ^{68}Ga-KR. Competitive blocking experiments further confirmed the in vivo dual-receptor targeting capability of ^{68}Ga-folate-KR. Collectively, our results highlight that ^{68}Ga-folate-KR enables more sensitive PET detection of ovarian cancer xenografts. With further optimization, dual-receptor-targeted radiotracers hold promise for clinical translation in both lesion detection and therapy response monitoring in ovarian cancer.

Keywords: Ovarian cancer, positron emission tomography, radiopharmaceuticals, molecular imaging, dual-targeting

Introduction

Ovarian cancer remains one of the most lethal gynecological malignancies worldwide, largely due to its high mortality rate and frequent diagnosis at late-stages [1, 2]. The disease typically presents with vague or nonspecific symptoms, leading to diagnosis at advanced stages in the majority of patients, where the 5-year survival rate falls below 30% [2, 3]. Current diagnostic approaches for ovarian cancer, such as pelvic ultrasound, CT, MRI, and serum biomarkers like cancer antigen 125 (CA-125) and human epididymis protein 4 (HE4), offer clinically useful information but suffer from limited sensitivity and specificity, particularly for early-stage disease [4, 5]. These limitations underscore the urgent need for more effective imaging strategies that enable early, accurate, and noninvasive detection of ovarian cancer. Timely and precise diagnosis can not only improve clinical outcomes but also guide surgical planning and support fertility-preserving interventions when appropriate.

The emergence of molecular imaging, particularly positron emission tomography (PET), has opened new avenues for noninvasive tumor characterization, early detection, and response monitoring [6, 7]. While ^{18}F-fluorodeoxyglucose (^{18}F-FDG) PET is widely used in oncology, including for ovarian cancer, its diagnostic performance is limited by its dependence on elevated glucose metabolism - a hallmark that is not exclusive to malignant cells and may also be observed in benign inflammatory or infectious processes [8]. Moreover, ^{18}F-FDG PET exhibits reduced sensitivity in detecting low-grade or mucinous ovarian cancers and can be confounded by physiological uptake in the intestines and reproductive organs, particularly in premenopausal women [9, 10]. These limitations highlight the pressing need for alternative PET radiotracers that selectively target molecular markers overexpressed in ovarian cancer, thereby enhancing diagnostic specificity and clinical accuracy.

Efforts to improve ovarian cancer imaging have focused on radiotracers targeting overexpressed cell-surface receptors. One of the most promising targets is folate receptor α (FRα), which is highly expressed in the majority of epithelial ovarian cancers while showing limited expression in normal tissues. A variety of FRα-targeted radiotracers, including folate derivatives labeled with radionuclides such as ^{99m}Tc, ^{111}In, ^{18}F, and ^{68}Ga, have shown encouraging results in both preclinical and early clinical studies [11-14]. Moreover, folate-conjugated fluorescent probes have been used intraoperatively to assist tumor visualization during surgery [15]. However, despite decades of research, FRα-targeted radiotracers have yet to achieve widespread clinical application, at least in part, due to their limited tumor accumulation and the variable expression of FRα across different histological subtypes of ovarian cancer.

https://doi.org/10.62347/IRKD4863

Beyond FRα, human epidermal growth factor receptor 2 (HER2) is another key molecular target under investigation for ovarian cancer imaging. HER2 is overexpressed in approximately 20-30% of ovarian cancers, particularly in serous, clear cell, and mucinous subtypes, and is often associated with poor prognosis [16, 17]. Various HER2-targeted PET imaging agents, including peptides, affibodies, and monoclonal antibodies, have been developed and evaluated across several tumor types [18-21]. Nevertheless, radiotracers targeting a single molecular marker may be insufficient due to tumor heterogeneity and variability in receptor expression [22]. To address these limitations, dual-targeting strategies that concurrently engage two distinct receptors offer a compelling alternative. Such approaches may enhance tumor detection sensitivity, improve radiotracer retention, and provide better tumor-to-background contrast by ensuring binding even when one of the targets is variably expressed [22, 23]. Recent studies have demonstrated that heterodimeric radiotracers can outperform their monovalent counterparts in various cancer models [24-26]. However, to our knowledge, no dual-receptor PET radiotracer targeting both FRα and HER2 has been systematically evaluated for PET imaging of ovarian cancer.

In this study, we developed a ^{68}Ga-labeled heterodimeric PET radiotracer that targets both FRα and HER2. The radiotracer incorporates a folate moiety and a HER2-binding peptide (denoted as the KR peptide; sequence: KLRLEWNR [27]), designed to enable concurrent binding to both receptors. We performed in vitro binding studies to confirm target specificity and conducted in vivo small-animal PET imaging in an ovarian cancer xenograft model to evaluate pharmacokinetics and tumor-targeting performance. Our findings provide preclinical proof-of-concept supporting the feasibility of dual-receptor PET imaging for ovarian cancer, with potential implications for early detection, patient stratification, and image-guided interventions.

Materials and methods

Reagents

The Lys-PEG4-folate (PEG4 = 15-amino-4,7,10,13-tetraoxapentadecanoic acid), PEG4-Lys(Dde)-Leu-Arg-Leu-Glu-Trp-Asn-Arg (PEG4-K(Dde)R), and the heterodimer Lys[PEG4-folate][PEG4-K(Dde)R] (Lys-2PEG4-folate-K(Dde)R) were custom synthesized by WuXi AppTec (Shanghai, China). DOTA-NHS-ester was purchased from Macrocyclics (Dallas, TX). ^{68}Ga was obtained from a ^{68}Ge/^{68}Ga generator (Isotope Technologies Garching GmbH, Germany) eluted with 0.1 N HCl. All water and buffers were passed through a Chelex 100 column prior to use to remove metal ions.

Transcriptomics analyses

The transcriptomics data for *FOLR1* (gene coding for FRα) and *HER2* (gene coding for HER2) were obtained from The Cancer Genome Atlas (TCGA) and Genotype-Tissue Expression (GTEx) project. All data were normalized using $\log2^{(TPM+1)}$ transformation, and expression levels were analyzed using the Gene Expression Profiling Interactive Analysis (GEPIA) platform [28].

DOTA conjugation

Lys-PEG4-folate, PEG4-K(Dde)R, and Lys-2PEG4-folate-K(Dde)R were conjugated with DOTA-NHS using a previously described method [24]. Briefly, each precursor was reacted with DOTA-NHS ester at a molar ratio of 1:5 in 0.1 M sodium bicarbonate buffer (pH 9.0) and stirred at 4°C for 4 h. The resulting DOTA-conjugated intermediates were purified by semi-preparative high-performance liquid chromatography (HPLC) to remove excess reagents and byproducts, followed by lyophilization. The Dde protecting group on the lysine side chain was then removed using 2% hydrazine in DMF (v/v) for 15 min at room temperature under gentle stirring. The deprotected products were further purified by semi-preparative HPLC, lyophilized, and characterized using matrix-assisted laser desorption/ionization time-of-flight mass spectrometry (MALDI-TOF-MS). DOTA-Lys-PEG4-folate was obtained in 62% yield with m/z 1203.5 for $[MH]^+$ ($C_{52}H_{78}N_{14}O_{19}$, calculated molecular weight 1202.6). DOTA-PEG4-KR was obtained in 56% yield with m/z 1747.9 for $[MH]^+$ ($C_{77}H_{130}N_{22}O_{24}$, calculated molecular weight 1747.0). DOTA-Lys-2PEG4-folate-KR was obtained in 65% yield with m/z 2546.1 for $[MH]^+$ ($C_{113}H_{180}N_{32}O_{35}$, calculated molecular weight 2545.3).

^{68}Ga radiolabeling

10 nmol of DOTA-Lys-PEG4-folate, DOTA-PEG4-KR, or DOTA-Lys-2PEG4-folate-KR was dissolved in 350 μL of 0.1 M sodium acetate buffer (pH 4.5) buffer and incubated with 370 MBq of $^{68}GaCl_3$ at 95°C for 15 min with constant agitation. The resulting compounds, ^{68}Ga-labled DOTA-Lys-PEG4-folate (^{68}Ga-folate), ^{68}Ga-labled DOTA-PEG4-KR (^{68}Ga-KR), and ^{68}Ga-labeled DOTA-Lys-2PEG4-folate-KR (^{68}Ga-folate-KR), were purified using analytical HPLC equipped with a radiation detector. The radioactive peaks containing the desired products were collected and rotary evaporated to remove the solvent. The products were formulated in phosphate-buffered saline (PBS), sterilized by passage through a 0.22-μm Millipore filter, and used for subsequent in vitro and in vivo studies. Radiochemical purity and in vitro stability were assessed in PBS or fetal bovine serum (FBS) at 0, 30, 60, and 120 min post-incubation using radio-HPLC.

Cell culture and animal models

SKOV3 human ovarian cancer and HEK293 human embryonic kidney cells were purchased from American Type Culture Collection (ATCC, Manassas, VA). Cells were cultured in Dulbecco's modified Eagle's medium (DMEM) supplemented with 10% FBS at 37°C in a humidified atmosphere containing 5% CO_2.

All animal procedures were approved by the Institutional Animal Care and Use Committee of Peking University Third Hospital. Female BALB/c nude mice (4-5 weeks old) were obtained from the Department of Experimental Animal, Peking University Health Science Center. The SKOV3 tumor-bearing mouse model was established by subcutaneous injection of 5×10^6 SKOV3 cells into the right flank. Tumor growth was monitored with caliper measurements, and tumor volume was calculated using the formula: volume = (length × width^2)/2.

Western blotting

Cells were lysed, and total protein concentrations were determined using a BCA assay kit (Thermo Fisher Scientific, Waltham, MA). Proteins were separated using sodium dodecyl sulfate-polyacrylamide gel electrophoresis and transferred onto polyvinylidene difluoride membranes. Membranes were blocked in 5% skimmed milk for 2 h, and then incubated overnight at 4°C with primary antibody against folate receptor 1 (60307-1-Ig; Proteintech, Chicago, IL) or HER2 primary antibody (60311-1-Ig; Proteintech). After washing with Tris-buffered saline containing 0.1% Tween-20, the membranes were incubated with horseradish peroxidase-conjugated secondary antibodies (Abclonal, Wuhan, China) for 1 h. Bands were visualized using a Tanon 5200 Multi imager and quantified using ImageJ (NIH, Bethesda, MD).

Flow cytometry and cell staining

The expression of FRα and HER2 on SKOV3 cells was assessed by flow cytometry and immunofluorescence staining. HEK293 cells were used as controls. For flow cytometry, cells were incubated with 5 μg/mL of anti-folate receptor 1 (60307-1-Ig; Proteintech) or anti-HER2 primary antibody (60311-1-Ig; Proteintech) for 1 h at room temperature. After washing with PBS, cells were incubated with fluorophore-conjugated secondary antibodies (Abclonal). Flow cytometry was performed using a BD cytometer (Becton Dickinson, Germany).

For cell staining, SKOV3 cells grown on 35 mm MatTek glass-bottom culture dishes were stained with 5 μg/mL of anti-folate receptor 1 (Proteintech) or anti-HER2 primary antibody (Proteintech) for 1 h at room temperature, followed by dye-labeled secondary antibodies. Cells were visualized using a confocal microscope (Leica, Wetzlar, Germany).

Cell binding assay

The receptor binding specificity of ^{68}Ga-folate, ^{68}Ga-KR, and ^{68}Ga-folate-KR was determined by in vitro cell binding assay. Briefly, SKOV3 cells were incubated with 74 kBq of each radiotracer with or without an excess dose (5 nmol) of cold competitor (Lys-PEG4-folate, PEG4-KR, Lys-2PEG4-folate-KR, or a combination of Lys-PEG4-folate and PEG4-KR). After incubation at 4°C for 2 h, cells were washed with PBS. Cells were then harvested, and cell-associated radioactivity was measured using a γ-counter (Packard, Meriden, CT). The results were expressed as the percentage of the total added dose per million cells (%AD/10^6 cells).

Small-animal PET imaging

Small-animal PET/CT imaging and image analysis were performed using a Super Nova small-animal PET/CT scanner (PINGSENG Healthcare, Shanghai, China). BALB/c nude mice bearing SKOV3 tumors (tumor volume: 200-300 mm^3) were intravenously injected with 5.55 MBq of either ^{68}Ga-folate, ^{68}Ga-KR, or ^{68}Ga-folate-KR. At 30, 60, and 120 min after injection of each radiotracer, 10-min static PET scanning was performed. For the blocking studies, mice were coinjected with 1 nmol of cold Lys-PEG4-folate, PEG4-KR, or Lys-PEG4-folate plus PEG4-KR along with 5.55 MBq of ^{68}Ga-folate-KR. Ten-min static PET scans were then acquired at 30 min after injection. For each PET scan, region-of-interest (ROIs) were drawn over the tumor and major organs, and the ROI-derived percentage injected dose per gram of tissue (%ID/g) was calculated as previously described [29, 30].

Biodistribution

Female BALB/c nude mice bearing subcutaneous SKOV3 tumors were injected with 3.7 MBq of ^{68}Ga-folate, ^{68}Ga-KR, or ^{68}Ga-folate-KR to evaluate the distribution of the radiotracers in the main organs. At 30, 60, and 120 min postinjection, mice were euthanized and blood, tumor, and main organs and tissues were collected, weighed, and measured using a γ-counter (Packard). The uptake of radiotracers were calculated and presented as %ID/g.

In vivo metabolic stability

To assess the in vivo metabolic stability of ^{68}Ga-folate-KR, female BALB/c normal mice were intravenously injected with 37 MBq of ^{68}Ga-folate-KR via the tail vein. At 30 min postinjection, serum and urine samples were collected and centrifuged. The supernatant was diluted with 50% aqueous acetonitrile, filtered through a 0.22-mm Millipore filter (Millipore, Billerica, MA), and analyzed by radio-HPLC.

Immunofluorescence staining

The expression of FRα and HER2 in tumor tissues was analyzed by immunofluorescence staining. Briefly, 5-μm-thick frozen tissue sections were fixed with ice-cold acetone and then blocked with 2% bovine serum albumin (in PBS) for 1 h. Tissues were then incubated with 10 μg/mL of anti-folate receptor 1 (Proteintech) or anti-HER2 primary antibody (Proteintech) for 1 h at room temperature, and then visualized with dye-labeled secondary antibodies under a confocal microscope (Leica).

Statistical analysis

Quantitative data are expressed as mean ± SD. Statistical analysis was performed using a one-way ANOVA and

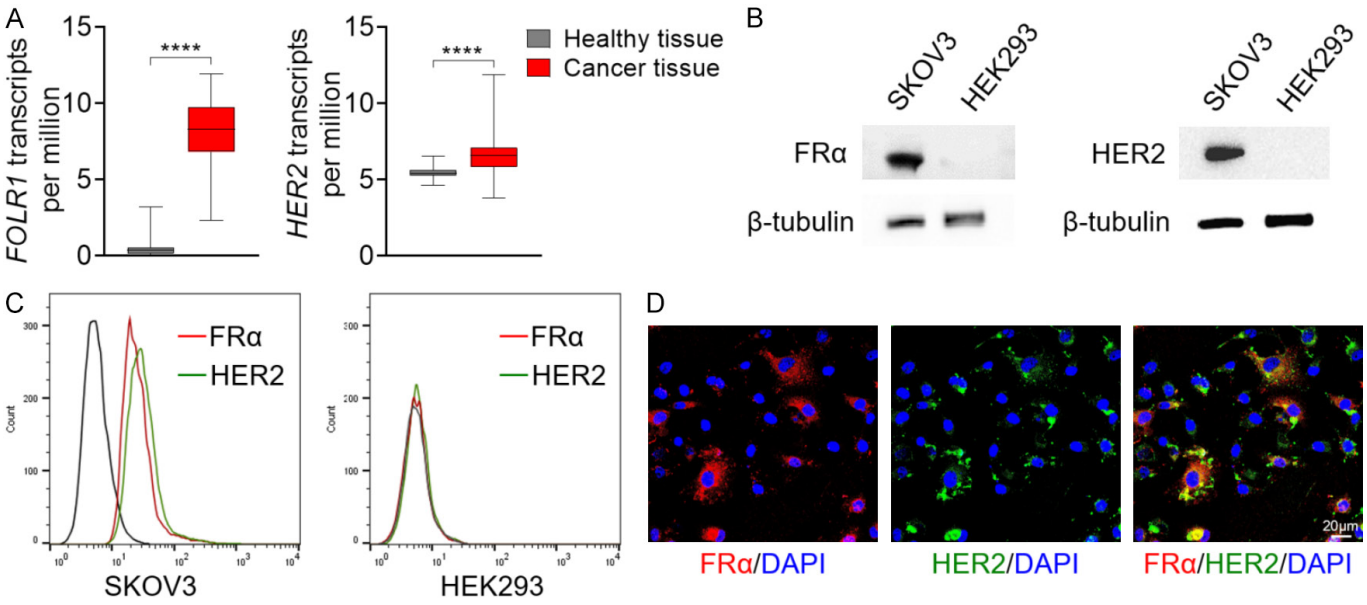

Figure 1. FRα and HER2 expression patterns of ovarian cancer and SKOV3 cells. A. Box plot comparing *FOLR1* and *HER2* messenger RNA expression levels in healthy ovarian tissues and ovarian cancer tissues. ****, $P < 0.0001$. B. Western blot analysis showing the expression of FRα and HER2 in SKOV3 cells. C. Flow cytometry analysis confirms co-expression of FRα and HER2 on SKOV3 cells. D. Immunofluorescence staining of SKOV3 cells demonstrates colocalization of FRα and HER2. Scale bar: 20 μm.

an unpaired Student's t test. *P* values of < 0.05 were considered statistically significant.

Results

Receptor expression patterns of ovarian cancer

Transcriptomics analysis of *FOLR1* and *HER2* (encoding FRα and HER2, respectively) revealed that both receptors are significantly upregulated in ovarian cancer tissues compared to normal ovarian tissues (**Figure 1A**), supporting the rationale for designing dual-targeted radiotracers against FRα and HER2. Based on these findings, we selected a SKOV3 ovarian cancer cell line for further in vitro studies. Dual expression of FRα and HER2 in SKOV3 cells was validated by Western blotting (**Figure 1B**), flow cytometry (**Figure 1C**), and immunofluorescence staining (**Figure 1D**).

Chemistry and radiochemistry

The DOTA conjugates of Lys-PEG4-folate, PEG4-KR, and Lys-2PEG4-folate-KR (**Figure 2A**) were confirmed by mass spectroscopy. The radiolabeling of ^{68}Ga was completed within 45 min, yielding a decay-corrected radiochemical yield of 90%-95%. After purification, the radiochemical purity of all three radiotracers exceeded 98%, with a specific activity of 30-40 MBq/nmol. ^{68}Ga-folate, ^{68}Ga-KR, and ^{68}Ga-folate-KR showed favorable in vitro stability, retaining over 80% radiochemical purity after 2 h of incubation in PBS or FBS (**Figure 2B-D**).

Cell binding assay

The binding specificity of ^{68}Ga-folate, ^{68}Ga-KR, and ^{68}Ga-folate-KR to the dual receptor-positive SKOV3 cells was confirmed by cell binding assay. The binding of ^{68}Ga-folate and ^{68}Ga-KR to SKOV3 cells was significantly inhibited by excess doses of Lys-PEG4-folate and PEG4-KR, respectively (**Figure 2E**, **2F**). Co-incubation with an excess of either Lys-PEG4-folate or PEG4-KR alone partially inhibited the binding of ^{68}Ga-folate-KR to SKOV3 cells, whereas co-incubation with both Lys-PEG4-folate and PEG4-KR, or with Lys-2PEG4-folate-KR almost completely abolished its binding (**Figure 2G**). These results indicate that ^{68}Ga-folate-KR binds specifically to both FRα and HER2 via receptor-mediated mechanisms, while ^{68}Ga-folate and ^{68}Ga-KR exhibit specificity for their respective single targets.

Small-animal PET imaging

Representative PET images at different time points postinjection of ^{68}Ga-folate, ^{68}Ga-KR, and ^{68}Ga-folate-KR in SKOV3 tumor-bearing mice are shown in **Figure 3A**. The SKOV3 tumors after injection of ^{68}Ga-folate, ^{68}Ga-KR, or ^{68}Ga-folate-KR were visible at 30 min postinjection, followed by signal clearance at 60 and 120 min postinjection. Prominent kidney uptake was observed for all radiotracers, indicating renal-urinary clearance. The ROI-derived tumor uptake of ^{68}Ga-folate-KR was determined to be 1.33 ± 0.08, 0.94 ± 0.13, and 0.55 ± 0.07 %ID/g at 30, 60, and 120 min postinjection, respectively, which are significantly higher than that of the monomeric radiotracers at corresponding time points ($P < 0.001$; **Figure 3B**). ^{68}Ga-folate-KR also showed elevated liver uptake at 30 min, which decreased to levels comparable with other radiotracers at later time points (**Figure 3C**). Renal accumulation was highest for ^{68}Ga-folate-KR across all time points (**Figure 3D**). Tumor-to-muscle and tumor-to-liver

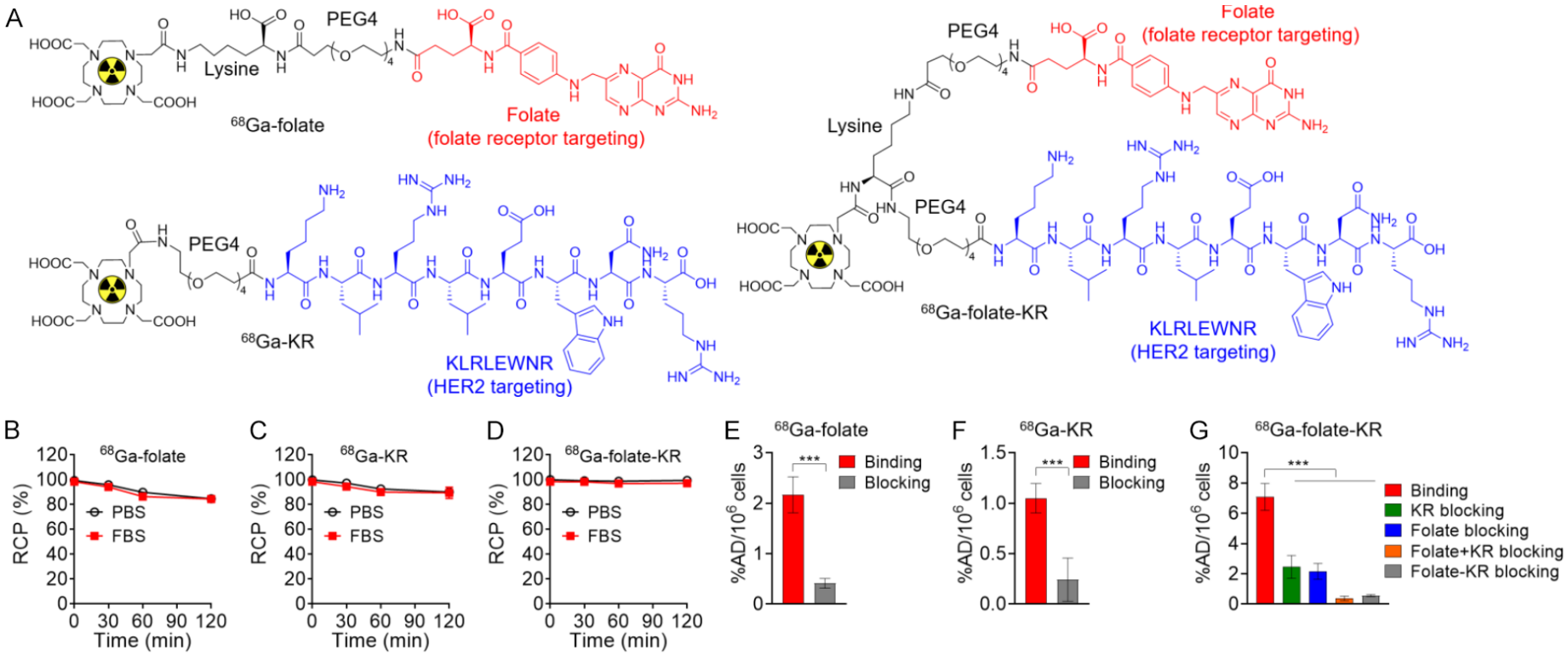

Figure 2. In vitro characterizations of ^{68}Ga-folate, ^{68}Ga-KR, and ^{68}Ga-folate-KR. (A) Chemical structures of ^{68}Ga-folate, ^{68}Ga-KR, and ^{68}Ga-folate-KR. (B-D) Radiochemical purity (RCP) values of ^{68}Ga-folate (B), ^{68}Ga-KR (C), and ^{68}Ga-folate-KR (D) after incubating for 0, 30, 60, and 120 min in PBS or FBS. (E) Competitive binding assay of ^{68}Ga-folate to SKOV3 cells in the presence of excess Lys-PEG4-folate. (F) Competitive binding assay of ^{68}Ga-KR to SKOV3 cells in the presence of excess PEG4-KR. (G) Competitive binding assay of ^{68}Ga-folate-KR to SKOV3 cells in the presence of excess PEG4-KR (KR), Lys-PEG4-folate (folate), Lys-PEG4-folate plus PEG4-KR (folate + KR), or Lys-2PEG4-folate-KR (folate-KR). All numerical data are presented as mean ± SD (n = 4). ***, $P < 0.001$.

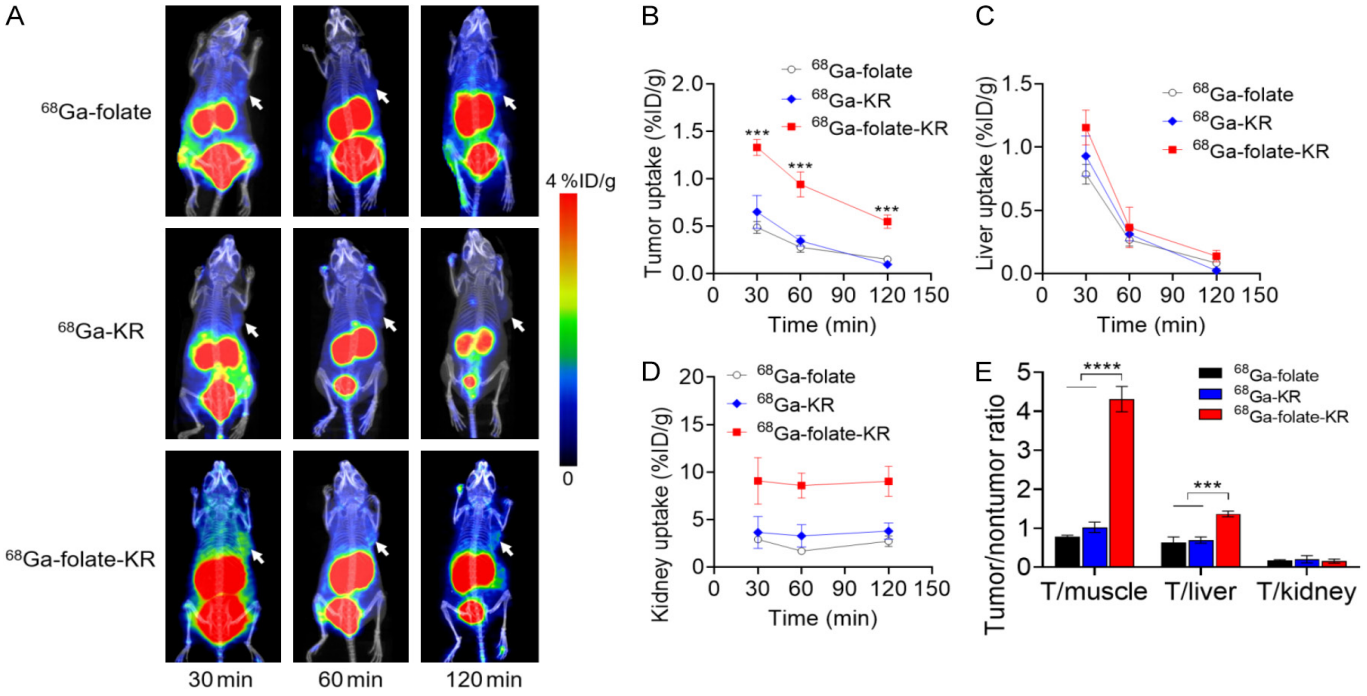

Figure 3. PET imaging of ^{68}Ga-folate, ^{68}Ga-KR, and ^{68}Ga-folate-KR. A. Representative PET/CT images of SKOV3 tumor-bearing mice at 30, 60, and 120 min after injection of ^{68}Ga-folate, ^{68}Ga-KR, and ^{68}Ga-folate-KR. Tumors are indicated by white arrows. B. Quantification of tumor uptake (%ID/g) at indicated time points. C. Liver uptake profiles of the three radiotracers. D. Kidney uptake kinetics of the three radiotracers. E. Tumor-to-muscle (T/muscle), tumor-to-liver (T/liver), and tumor-to-kidney (T/kidney) uptake ratios of the radiotracers at 30 min postinjection. All numerical data are presented as mean ± SD (n = 4 per group). ***, $P < 0.001$; ****, $P < 0.0001$.

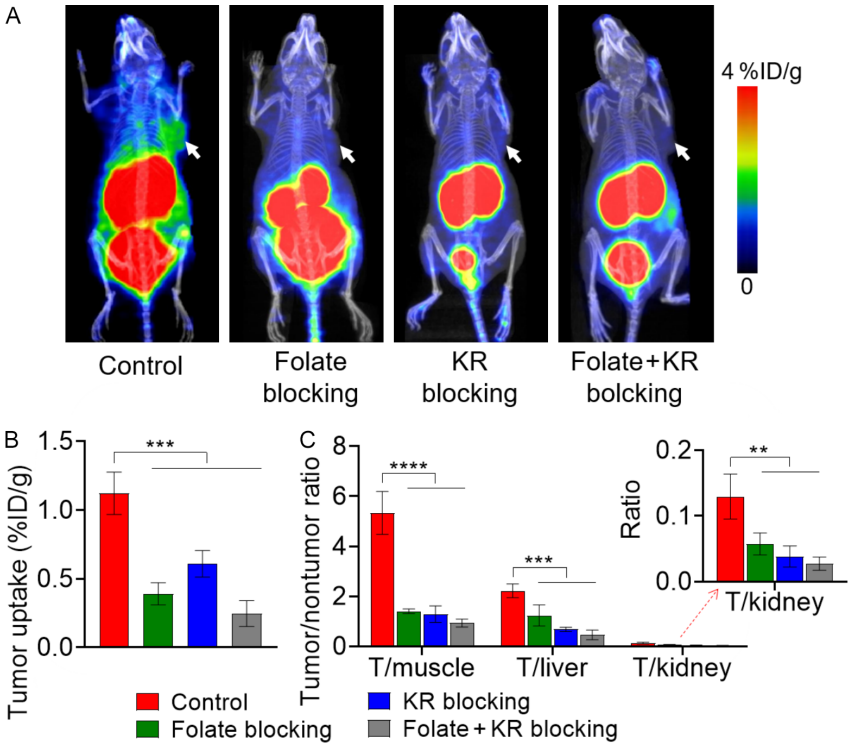

Figure 4. PET imaging of ^{68}Ga-folate-KR with or without blocking. A. Representative PET/CT images showing receptor blocking effects on ^{68}Ga-folate-KR uptake in SKOV3 tumors following co-injection with excess Lys-PEG4-folate (folate), PEG4-KR (KR), or Lys-PEG4-folate plus PEG4-KR (folate + KR). Tumors are indicated by white arrows. B. Tumor uptake quantification (%ID/g) in each blocking group. C. Quantified tumor-to-muscle (T/muscle), tumor-to-liver (T/liver), and tumor-to-kidney (T/kidney) ratios of ^{68}Ga-folate-KR under blocking conditions. All numerical data are presented as mean ± SD (n = 4 per group). **, $P < 0.01$; ***, $P < 0.001$; ****, $P < 0.0001$.

ratios of ^{68}Ga-folate-KR were also significantly higher than that of ^{68}Ga-folate and ^{68}Ga-KR at 30 min postinjection (**Figure 3E**).

The in vivo FRα and HER2 dual receptor-binding capability of ^{68}Ga-folate-KR was confirmed by several blocking studies (**Figure 4A**). The tumor uptake of ^{68}Ga-folate-KR was only partially reduced by excess folate (from 1.12 ± 0.15 %ID/g to 0.39 ± 0.08 %ID/g) or KR (from 1.12 ± 0.15 %ID/g to 0.61 ± 0.09 %ID/g) blocking. However, the tumor uptake of ^{68}Ga-folate-KR was nearly abolished when both excess Lys-PEG4-folate and PEG4-KR were co-injected (from 1.12 ± 0.15 %ID/g to 0.24 ± 0.09 %ID/g) (**Figure 4B**). The tumor-to-muscle, tumor-to liver, and tumor-to-kidney ratios of ^{68}Ga-folate-KR was also significantly blocked by Lys-PEG4-folate plus PEG4-KR (**Figure 4C**).

Biodistribution studies

Biodistribution profiles of the ^{68}Ga-folate, ^{68}Ga-KR, and ^{68}Ga-folate-KR were examined in SKOV3 tumor-bearing nude mice. As shown in **Figure 5A-C**, predominant kidney uptake was observed for all three radiotracers, which is consistent with

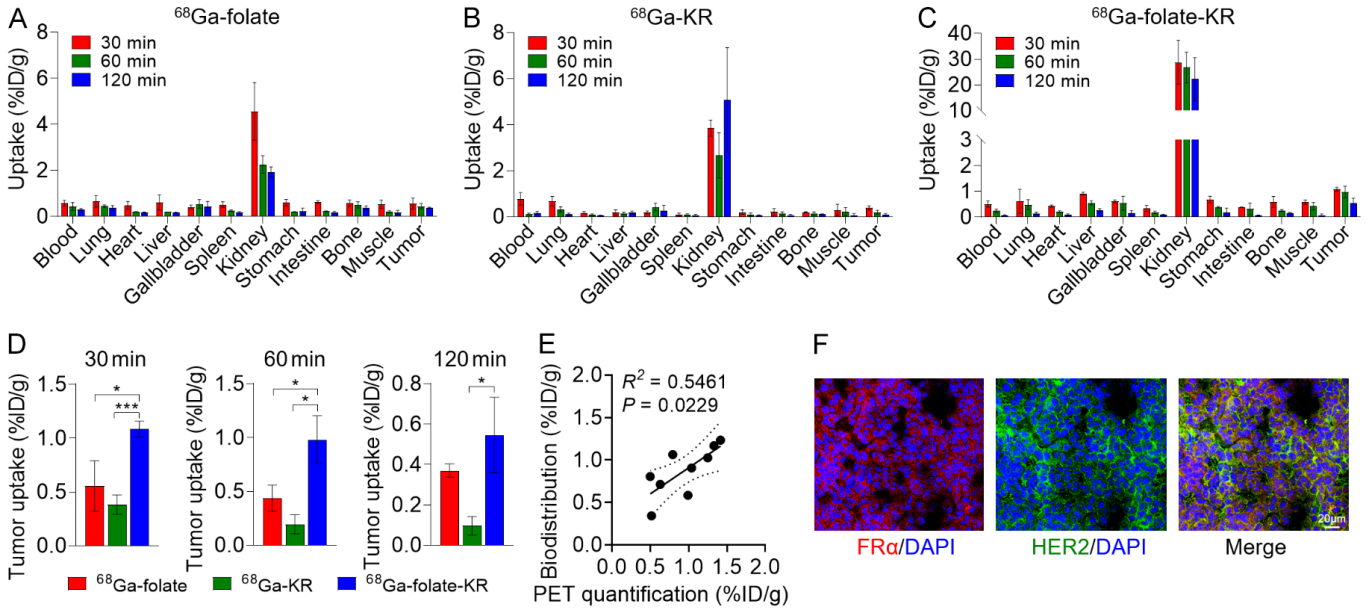

Figure 5. Biodistribution of ^{68}Ga-folate, ^{68}Ga-KR, and ^{68}Ga-folate-KR and ex vivo validate of FRα and HER2 expression in tumor tissues. (A-C) Biodistribution of ^{68}Ga-folate (A), ^{68}Ga-KR (B), and ^{68}Ga-folate-KR (C) in SKOV3 tumor-bearing BALB/c nude mice at 30, 60, and 120 min postinjection. (D) Comparison of tumor uptake between dual- and mono-targeted radiotracers at different time points. *, $P < 0.05$; ***, $P < 0.001$. All numerical data are presented as mean ± SD (n = 4 per group). (E) Correlation between PET-derived and ex vivo biodistribution-derived tumor uptake values of ^{68}Ga-folate-KR. (F) Immunofluorescence staining of FRα and HER2 for the SKOV-3 tumors harvested from BALB/c nude mice. Scale bar, 20 μm.

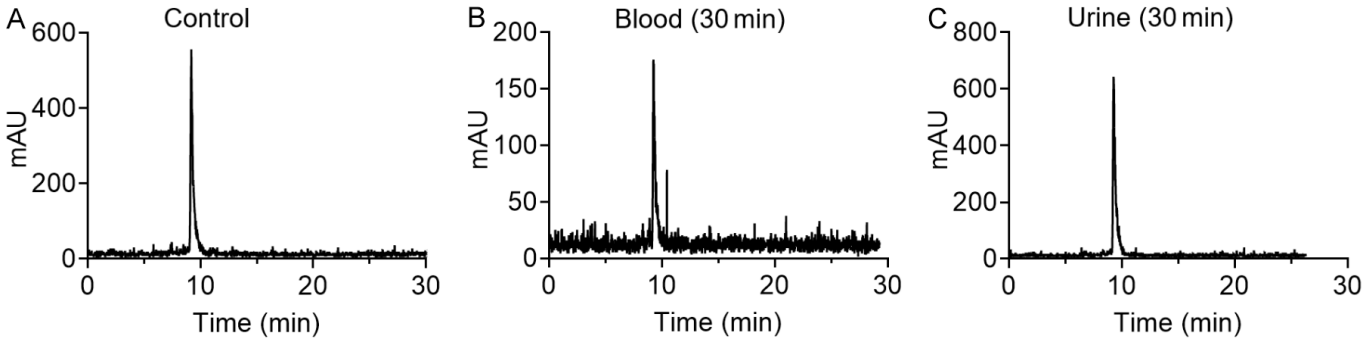

Figure 6. Metabolic stability of ^{68}Ga-folate-KR analyzed by HPLC. (A) HPLC chromatogram of purified ^{68}Ga-folate-KR. (B, C) Representative HPLC chromatograms of mouse serum (B) and urine (C) collected 30 min after intravenous injection of ^{68}Ga-folate-KR in BALB/c mice. Data are representative of three independent experiments.

the results observed in PET imaging (**Figure 3A**). The tumor uptake of ^{68}Ga-folate-KR was significantly higher than that of ^{68}Ga-folate and ^{68}Ga-KR at all examined time points (**Figure 5D**), confirming the improved tumor uptake of the dual receptor targeting radiotracer. A positive correlation was found between tumor uptake values obtained from PET imaging and ex vivo biodistribution (**Figure 5E**), supporting the quantitative accuracy of noninvasive PET imaging for evaluating in vivo radiotracer behavior. Ex vivo histological staining validated the co-expression of FRα and HER2 in SKOV3 tumor tissues (**Figure 5F**).

Metabolic stability of ^{68}Ga-folate-KR

The metabolic stability of ^{68}Ga-folate-KR in mice serum and urine at 30 min after injection were determined by HPLC. As shown in **Figure 6A-C**, both the serum and urine detected minimal detectable metabolite formation, indicating that ^{68}Ga-folate-KR possesses excellent metabolic stability in vivo.

Discussion

Tumor receptor-targeted PET imaging has emerged as a powerful tool in precision oncology, enabling noninvasive visualization of tumor-associated biomarkers to facilitate early diagnosis, patient stratification, and real-time monitoring of therapeutic response [31]. Most clinically employed PET radiotracers are designed to target a single receptor, providing valuable information on receptor expression and guiding receptor-targeted therapies. However, the diagnostic performance of single-receptor targeting can be limited by the inherent heterogeneity of tumors [32]. Loss or downregulation of a single receptor,

which is common in advanced or treatment-resistant tumors, may lead to false-negative results, thereby reducing diagnostic sensitivity and compromising clinical decision-making. To address these limitations, dual-targeting strategies have gained increasing interest as a means to enhance radiotracer accumulation, increase binding avidity, and expand the spectrum of detectable lesions [33, 34]. In this study, we developed and evaluated a heterodimeric PET radiotracer, ^{68}Ga-folate-KR, designed to simultaneously target FRα and HER2, two clinically relevant targets frequently co-expressed in ovarian cancer. Our data demonstrate that ^{68}Ga-folate-KR retains high specificity and affinity for both targets, offering a promising alternative to ^{18}F-FDG by enabling more selective PET imaging of ovarian cancer.

Folate-based PET radiotracers have long been explored for ovarian cancer imaging due to the overexpression of FRα in many epithelial ovarian carcinomas [35, 36]. However, the clinical translation of radiolabeled folate analogs has been hampered, at least in part, by their suboptimal tumor uptake and unfavorable pharmacokinetics. Consistent with previous studies [37, 38], our PET imaging of the monomeric ^{68}Ga-folate revealed limited tumor accumulation (**Figure 3**), underscoring the need for enhanced targeting strategies. By incorporating the HER2-targeting KR peptide, we generated a heterodimeric radiotracer with significantly improved tumor uptake and tumor-to-background contrast in the SKOV3 xenograft model, as confirmed by PET imaging and ex vivo biodistribution studies. A series of in vitro and in vivo blocking experiments further validated the specific binding of ^{68}Ga-folate-KR to both FRα and HER2. These findings support the dual-targeting capability of ^{68}Ga-folate-KR and suggest its potential to detect tumors expressing either target alone.

Despite these improvements, the absolute tumor uptake of ^{68}Ga-folate-KR remained moderate, and kidney accumulation was relatively high. These limitations may result from the intrinsic affinities of the individual ligands and rapid renal clearance. Therefore, further molecular optimization is warranted to fully realize the potential of this dual-targeting approach. For instance, replacing folate with 5-methyltetrahydrofolate (MTHF), a derivative with higher specificity and binding affinity for FRα [12], could improve receptor targeting efficiency. Similarly, chemical modifications to the KR peptide, such as cyclization or the incorporation of D-amino acid, may enhance HER2 binding affinity and proteolytic resistance, ultimately improving tumor retention [39, 40].

In addition to optimizing binding affinity and enzymatic resistance, pharmacokinetic properties of the radiotracer could be tuned through various structure modification strategies. These include the incorporation of hydrophilic linkers to reduce off-target accumulation, multimerization to increase valency [41, 42], conjugation with albumin-binding moieties to prolong circulation half-life [43, 44], and enzymolysis-based clearance mechanisms to facilitate rapid renal clearance [45, 46]. Notable, despite the moderate affinities of folate and KR as monovalent ligands, their combination in the heterodimeric format synergistically improved in tumor targeting, highlighting the value of dual-receptor engagement in enhancing PET imaging performance.

Beyond FRα and HER2, several alternative molecular targets have shown promise in ovarian cancer imaging, including fibroblast activation protein (FAP) [47] and poly(ADP-ribose) polymerase-1 (PARP1) [48]. The modularity of the heterodimer design allows for flexible replacement or combination of different targeting ligands, enabling the development of customized PET radiotracers tailored to specific tumor phenotypes. Integration of transcriptomic, proteomic, and spatial profiling data from patient-derived tumor samples could further guide the rational selection of dual- or multi-targeting strategies.

Peptide-based radiotracers are generally characterized by low immunogenicity and favorable safety profiles. Several such radiotracers, including radiolabeled heterodimeric peptides, have been evaluated in clinical studies without reports of significant immune responses or adverse events [49, 50]. These observations support the translational potential of heterodimeric PET radiotracers and underscore their promise as next-generation agents for precision oncology.

Conclusion

We synthesized and evaluated a new PET radiotracer, ^{68}Ga-folate-KR, capable of concurrently targeting FRα and HER2 in an ovarian cancer mouse model. This dual-targeted radiotracer demonstrated high specificity for both receptors, robust in vivo stability, and markedly enhanced tumor PET imaging compared to its monovalent analogs. Our results highlight the potential of dual-receptor PET imaging to address the challenges posed by receptor heterogeneity in ovarian cancer. Further refinement of ^{68}Ga-folate-KR could pave the way for its clinical application as a precision PET imaging agent in the management of ovarian malignancies.

Acknowledgements

This work was supported by the National Key R&D Program of China (2024YFA1014102) and the Key Clinical Project of Peking University Third Hospital (BYSYZD-2024005 and BYSYZD2023016).

Disclosure of conflict of interest

None.

Address correspondence to: Dr. Rong Li, Department of Obstetrics and Gynecology, Peking University Third Hospital, Beijing 100191, China. E-mail: roseli001@sina.com

References

[1] Kordowitzki P, Lange B, Elias KM, Haigis MC, Mechsner S, Braicu IE and Sehouli J. Transforming treatment paradigms: focus on personalized medicine for high-grade serous ovarian cancer. CA Cancer J Clin 2025; [Epub ahead of print].

[2] Torre LA, Trabert B, DeSantis CE, Miller KD, Samimi G, Runowicz CD, Gaudet MM, Jemal A and Siegel RL. Ovarian cancer statistics, 2018. CA Cancer J Clin 2018; 68: 284-296.

[3] Stewart C, Ralyea C and Lockwood S. Ovarian cancer: an integrated review. Semin Oncol Nurs 2019; 35: 151-156.

[4] Sharma SK, Nemieboka B, Sala E, Lewis JS and Zeglis BM. Molecular imaging of ovarian cancer. J Nucl Med 2016; 57: 827-833.

[5] Scholler N and Urban N. CA125 in ovarian cancer. Biomark Med 2007; 1: 513-523.

[6] James ML and Gambhir SS. A molecular imaging primer: modalities, imaging agents, and applications. Physiol Rev 2012; 92: 897-965.

[7] Juweid ME, Al-Qasem SF, Khuri FR, Gallamini A, Lohmann P, Ziellenbach HJ and Mottaghy FM. Beyond fluorodeoxyglucose: molecular imaging of cancer in precision medicine. CA Cancer J Clin 2025; 75: 226-242.

[8] Tagliabue L and Del Sole A. Appropriate use of positron emission tomography with [18F]fluorodeoxyglucose for staging of oncology patients. Eur J Intern Med 2014; 25: 6-11.

[9] Delgado Bolton RC, Aide N, Colletti PM, Ferrero A, Paez D, Skanjeti A and Giammarile F. EANM guideline on the role of 2-[18F]FDG PET/CT in diagnosis, staging, prognostic value, therapy assessment and restaging of ovarian cancer, endorsed by the American College of Nuclear Medicine (ACNM), the Society of Nuclear Medicine and Molecular Imaging (SNMMI) and the International Atomic Energy Agency (IAEA). Eur J Nucl Med Mol Imaging 2021; 48: 3286-3302.

[10] Lee EYP, Philip Ip PC, Tse KY, Kwok ST, Chiu WK and Ho G. PET/computed tomography transformation of oncology: ovarian cancers. PET Clin 2024; 19: 207-216.

[11] Houson HA, Wu Z, Cao PD, Lindsey JS and Lapi SE. Customizable porphyrin platform enables folate receptor PET imaging using copper-64. Mol Pharm 2024; 21: 2441-2455.

[12] Guzik P, Fang HY, Deberle LM, Benešová M, Cohrs S, Boss SD, Ametamey SM, Schibli R and Müller C. Identification of a PET radiotracer for imaging of the folate receptor-α: a potential tool to select patients for targeted tumor therapy. J Nucl Med 2021; 62: 1475-1481.

[13] Ruytenberg T, Ciggaar IA, Peters ITA, Noortman WA, Dibbets-Schneider P, de Muynck LDAN, Kuil J, de Kroon CD, Molenaar TJM, Helmerhorst HJF, Pereira Arias-Bouda LM, Vahrmeijer AL, Windhorst AD, van Velden FHP, Gaarenstroom KN and de Geus-Oei LF. Challenges in pharmacokinetic modelling of [18F]fluoro-PEG-folate PET/CT imaging in epithelial ovarian cancer patients. Mol Imaging Biol 2024; 26: 577-584.

[14] Chen Q, Meng X, McQuade P, Rubins D, Lin SA, Zeng Z, Haley H, Miller P, González Trotter D and Low PS. Folate-PEG-NOTA-Al18F: a new folate based radiotracer for PET imaging of folate receptor-positive tumors. Mol Pharm 2017; 14: 4353-4361.

[15] van Dam GM, Themelis G, Crane LM, Harlaar NJ, Pleijhuis RG, Kelder W, Sarantopoulos A, de Jong JS, Arts HJ, van der Zee AG, Bart J, Low PS and Ntziachristos V. Intraoperative tumor-specific fluorescence imaging in ovarian cancer by folate receptor-α targeting: first in-human results. Nat Med 2011; 17: 1315-1319.

[16] Yoon J and Oh DY. HER2-targeted therapies beyond breast cancer - an update. Nat Rev Clin Oncol 2024; 21: 675-700.

[17] Iqbal N and Iqbal N. Human epidermal growth factor receptor 2 (HER2) in cancers: overexpression and therapeutic implications. Mol Biol Int 2014; 2014: 852748.

[18] Jiang D, Im HJ, Sun H, Valdovinos HF, England CG, Ehlerding EB, Nickles RJ, Lee DS, Cho SY, Huang P and Cai W. Radiolabeled pertuzumab for imaging of human epidermal growth factor receptor 2 expression in ovarian cancer. Eur J Nucl Med Mol Imaging 2017; 44: 1296-1305.

[19] Guo X, Liang X, Li B, Mao Y, Zhou N, Liu J, Yang G, Wang Z, Song G and Yang Z. Al18F-NOTA-HER2-BCH versus 18F-FDG PET/CT in evaluating newly diagnosed HER2-low breast cancer patients. Eur J Nucl Med Mol Imaging 2025; [Epub ahead of print].

[20] Guo X, Xu C, Zhu X, Wang X, Hao Y, Wang X, Yao Y, Fang J and Wang K. In silico design and evaluation of novel peptide-based PET probe for noninvasive imaging of HER2 expression in breast cancer. J Med Chem 2025; 68: 10461-10472.

[21] Yeh R, Pareja F, Shobeiri P, Ross D, Jayaprakasam VS, Razmaria AA, Drago JZ, Mauguen A, Lyashchenko SK, Zeglis BM, Lewis JS and Ulaner GA. Detection of HER2-low lesions using HER2-targeted PET imaging in patients with metastatic breast cancer: a paired HER2 PET and tumor biopsy analysis. J Nucl Med 2025; 66: 873-879.

[22] Liu Z and Wang F. Dual-targeted molecular probes for cancer imaging. Curr Pharm Biotechnol 2010; 11: 610-619.

[23] Ehlerding EB, Sun L, Lan X, Zeng D and Cai W. Dual-targeted molecular imaging of cancer. J Nucl Med 2018; 59: 390-395.

[24] Liu Z, Li ZB, Cao Q, Liu S, Wang F and Chen X. Small-animal PET of tumors with 64Cu-labeled RGD-bombesin heterodimer. J Nucl Med 2009; 50: 1168-1177.

[25] Chen L, Cheng S, Zhu D, Bao G, Wang Z, Deng X, Liu X, Ma X, Zhao J, Zhu L and Zhu X. Synthesis and preclinical evaluation of dual-specific probe targeting glypican-3 and prostate-specific membrane antigen for hepatocellular carcinoma PET imaging. Mol Pharm 2025; 22: 209-220.

[26] Wang X, Zhang X, Zhang X, Guan L, Gao X, Xu L, Pang H, Du J, Zhang J and Cui M. Design, preclinical evaluation, and first-in-human PET study of [68Ga]Ga-PSFA-01: a PSMA/FAP heterobivalent tracer. Eur J Nucl Med Mol Imaging 2025; 52: 1166-1176.

[27] Wang Z, Wang W, Bu X, Wei Z, Geng L, Wu Y, Dong C, Li L, Zhang D, Yang S, Wang F, Lausted C, Hood L and Hu Z. Microarray based screening of peptide nano probes for HER2 positive tumor. Anal Chem 2015; 87: 8367-8372.

[28] Tang Z, Li C, Kang B, Gao G, Li C and Zhang Z. GEPIA: a web server for cancer and normal gene expression profiling and interactive analyses. Nucleic Acids Res 2017; 45: W98-W102.

[29] Du J, Han S, Zhou H, Wang J, Wang F, Zhao M, Song R, Li K, Zhu H, Zhang W, Yang Z and Liu Z. Targeted protein degradation combined with PET imaging reveals the role of host PD-L1 in determining anti-PD-1 therapy efficacy. Eur J Nucl Med Mol Imaging 2024; 51: 3559-3571.

[30] Liu N, Yang X, Gao C, Wang J, Zeng Y, Zhang L, Yin Q, Zhang T, Zhou H, Li K, Du J, Zhou S, Zhao X, Zhu H, Yang Z and Liu Z. Noninvasively deciphering the immunosuppressive tumor microenvironment using galectin-1 PET to inform immunotherapy responses. J Nucl Med 2024; 65: 728-734.
[31] Mankoff DA, Link JM, Linden HM, Sundararajan L and Krohn KA. Tumor receptor imaging. J Nucl Med 2008; 49 Suppl 2: 149S-163S.
[32] Zhang C, Guan Y, Sun Y, Ai D and Guo Q. Tumor heterogeneity and circulating tumor cells. Cancer Lett 2016; 374: 216-223.
[33] Taghipour YD, Zarebkohan A, Salehi R, Rahimi F, Torchilin VP, Hamblin MR and Seifalian A. An update on dual targeting strategy for cancer treatment. J Control Release 2022; 349: 67-96.
[34] Liu N, Wan Q, Wu X, Zhao T, Jakobsson V, Yuan H, Chen X, Zhang J and Zhang W. A comparison of [18F]AlF- and 68Ga-labeled dual targeting heterodimer FAPI-RGD in malignant tumor: preclinical evaluation and pilot clinical PET/CT imaging. Eur J Nucl Med Mol Imaging 2024; 51: 1685-1697.
[35] Boss SD and Ametamey SM. Development of folate receptor-targeted PET radiopharmaceuticals for tumor imaging-a bench-to-bedside journey. Cancers (Basel) 2020; 12: 1508.
[36] Müller C. Folate-based radiotracers for PET imaging--update and perspectives. Molecules 2013; 18: 5005-5031.
[37] Feng J, Zhang X, Jiang Y, Wang Q, Ruan Q, Yin G, Han P, Du J and Zhang J. Development of a novel 99mTc-labeled folate derivative containing phenyl isonitrile to target folate receptor with reduced renal uptake. Mol Pharm 2024; 21: 5681-5689.
[38] Müller C, Schibli R, Krenning EP and de Jong M. Pemetrexed improves tumor selectivity of 111In-DTPA-folate in mice with folate receptor-positive ovarian cancer. J Nucl Med 2008; 49: 623-629.
[39] Wu Y, Li L, Wang Z, Shi J, Hu Z, Gao S, Miao W, Ma Q, Dong C and Wang F. Imaging and monitoring HER2 expression in breast cancer during trastuzumab therapy with a peptide probe (99m)Tc-HYNIC-H10F. Eur J Nucl Med Mol Imaging 2020; 47: 2613-2623.
[40] Shi J, Du S, Wang R, Gao H, Luo Q, Hou G, Zhou Y, Zhu Z and Wang F. Molecular imaging of HER2 expression in breast cancer patients using a novel peptide-based tracer (99m)Tc-HP-Ark2: a pilot study. J Transl Med 2023; 21: 19.
[41] Cossu J, Thoreau F and Boturyn D. Multimeric RGD-based strategies for selective drug delivery to tumor tissues. Pharmaceutics 2023; 15: 525.
[42] Shi J, Wang F and Liu S. Radiolabeled cyclic RGD peptides as radiotracers for tumor imaging. Biophys Rep 2016; 2: 1-20.
[43] Lau J, Jacobson O, Niu G, Lin KS, Bénard F and Chen X. Bench to bedside: albumin binders for improved cancer radioligand therapies. Bioconjug Chem 2019; 30: 487-502.
[44] Liu Z and Chen X. Simple bioconjugate chemistry serves great clinical advances: albumin as a versatile platform for diagnosis and precision therapy. Chem Soc Rev 2016; 45: 1432-1456.
[45] Zhang M, Kang F, Xing T, Wang J, Ma T, Li G, Quan Z, Yang W, Chen X and Wang J. First-in-human validation of enzymolysis clearance strategy for decreasing renal radioactivity using modified [68Ga]Ga-HER2 affibody. Eur J Nucl Med Mol Imaging 2024; 51: 1713-1724.
[46] Zhang M, Ye J, Xie Z, Yan Y, Wang J and Chen X. Optimization of enzymolysis clearance strategy to enhance renal clearance of radioligands. Bioconjug Chem 2021; 32: 2108-2116.
[47] Florit A, de Koster EJ, Sassano S, Alic L, Pisano G, van Velden FHP, Annunziata S, Primac I, Ruggiero MR, Müller C, Sala E, Fendler WP, Scambia G, de Geus-Oei LF, Fagotti A, Rufini V and Collarino A. Head-to-head comparison of fibroblast activation protein inhibitors (FAPI) radiopharmaceuticals and [18F]FDG in gynaecological malignancies: systematic literature review and meta-analysis. Eur J Nucl Med Mol Imaging 2025; [Epub ahead of print].
[48] Weeks JK, Pantel AR, Gitto SB, Liu F, Schubert EK, Pryma DA, Farwell MD, Mankoff DA, Mach RH, Simpkins F and Lin LL. [18F]Fluorthanatrace PET in ovarian cancer: comparison with [18F]FDG PET, lesion location, tumor grade, and breast cancer gene mutation status. J Nucl Med 2025; 66: 34-39.
[49] Zhao L, Wen X, Xu W, Pang Y, Sun L, Wu X, Xu P, Zhang J, Guo Z, Lin Q, Chen X and Chen H. Clinical evaluation of 68Ga-FAPI-RGD for imaging of fibroblast activation protein and integrin αvβ3 in various cancer types. J Nucl Med 2023; 64: 1210-1217.
[50] Wen X, Wang R, Xu P, Shi M, Shang Q, Zeng X, Zeng X, Liu J, Wang X, Zhu Z, Guo Z, Chen X and Zhang J. Synthesis, preclinical, and initial clinical evaluation of integrin αvβ3 and gastrin-releasing peptide receptor (GRPR) dual-targeting radiotracer [68Ga]Ga-RGD-RM26-03. Eur J Nucl Med Mol Imaging 2024; 51: 2023-2035.